View metadata, citation and similar papers at core.ac.uk

brought to you by CORE

provided by UNL | Libraries

University of Nebraska - Lincoln

DigitalCommons@University of Nebraska - Lincoln

Faculty Publications, Department of Physics and Astronomy

Research Papers in Physics and Astronomy

2010

Identification of electron and hole traps in lithium tetraborate ($Li_2B_4O_7$) crystals: Oxygen vacancies and lithium vacancies

M. W. Swinney

J. W. McClory

J. C. Petrosky

Shan Yang (??)

A. T. Brant

See next page for additional authors

Follow this and additional works at: https://digitalcommons.unl.edu/physicsfacpub

This Article is brought to you for free and open access by the Research Papers in Physics and Astronomy at DigitalCommons@University of Nebraska - Lincoln. It has been accepted for inclusion in Faculty Publications, Department of Physics and Astronomy by an authorized administrator of DigitalCommons@University of Nebraska - Lincoln.

Authors

M. W. Swinney, J. W. McClory, J. C. Petrosky, Shan Yang (??), A. T. Brant, V. T. Adamiv, Ya. V. Burak, P. A. Dowben, and L. E. Halliburton

Identification of electron and hole traps in lithium tetraborate ($Li_2B_4O_7$) crystals: Oxygen vacancies and lithium vacancies

M. W. Swinney,[1] J. W. McClory,[1,a)] J. C. Petrosky,[1] Shan Yang (杨山),[2] A. T. Brant,[2] V. T. Adamiv,[3] Ya. V. Burak,[3] P. A. Dowben,[4] and L. E. Halliburton[2]
[1]*Department of Engineering Physics, Air Force Institute of Technology, Wright-Patterson Air Force Base, Ohio 45433, USA*
[2]*Department of Physics, West Virginia University, Morgantown, West Virginia 26506, USA*
[3]*Institute of Physical Optics, Dragomanov 23, L'viv 79005, Ukraine*
[4]*Department of Physics and Astronomy, Nebraska Center for Materials and Nanoscience, University of Nebraska, Lincoln, Nebraska 68588, USA*

(Received 7 January 2010; accepted 18 March 2010; published online 11 June 2010)

Electron paramagnetic resonance (EPR) and electron-nuclear double resonance (ENDOR) are used to identify and characterize electrons trapped by oxygen vacancies and holes trapped by lithium vacancies in lithium tetraborate ($Li_2B_4O_7$) crystals. Our study includes a crystal with the natural abundances of ^{10}B and ^{11}B and a crystal highly enriched with ^{10}B. The as-grown crystals contain isolated oxygen vacancies, lithium vacancies, and copper impurities, all in nonparamagnetic charge states. During an irradiation at 77 K with 60 kV x-rays, doubly ionized oxygen vacancies trap electrons while singly ionized lithium vacancies and monovalent copper impurities trap holes. The vacancies return to their preirradiation charge states when the temperature of the sample is increased to approximately 90 K. Hyperfine interactions with ^{10}B and ^{11}B nuclei, observed between 13 and 40 K in the radiation-induced EPR and ENDOR spectra, provide models for the two vacancy-related defects. The electron trapped by an oxygen vacancy is localized primarily on only one of the two neighboring boron ions while the hole stabilized by a lithium vacancy is localized on a neighboring oxygen ion with nearly equal interactions with the two boron ions adjacent to the oxygen ion.
© *2010 American Institute of Physics*. [doi:10.1063/1.3392802]

I. INTRODUCTION

Lithium tetraborate ($Li_2B_4O_7$) is a versatile insulating crystal with important electrical, optical, and mechanical properties. Applications include nonlinear optics, radiation dosimetry, and bulk and surface acoustic wave devices. A large optical gap (transparency extending to 170 nm at room temperature) and appropriate birefringence make this material suitable for frequency conversion of lasers (i.e., harmonic generation) from the visible to the ultraviolet regions of the spectrum.[1–3] Thermoluminescence peaks associated with Cu or Ag dopants occur above room temperature and make $Li_2B_4O_7$ a tissue-equivalent radiation dosimeter.[4–6] Also, $Li_2B_4O_7$ may be used as a neutron dosimeter since two of its naturally occurring nuclei (^6Li and ^{10}B) have large cross sections for thermal neutron capture.[7] The mechanical properties of $Li_2B_4O_7$, e.g., moderately large piezoelectric constants and zero temperature coefficients of frequency and delay, make these crystals suitable for signal processing, transducer, and frequency control devices.[8–10] $Li_2B_4O_7$ also has an appreciable pyroelectric coefficient and thus may be used as a thermal sensor.[11,12]

Many of the optical and dosimetry applications of $Li_2B_4O_7$ crystals are significantly affected by the presence of point defects. Native defects (i.e., cation and anion vacancies) and impurities are expected in these crystals. A recent combined photoemission and inverse photoemission study provides supporting evidence for the presence of defects by suggesting that the Fermi level in nominally undoped $Li_2B_4O_7$ crystals is above the middle of the band gap.[13] Vacancy formation may result from nonstoichiometric growth conditions or from the volatility of constituents during growth. Impurities, on the other hand, may be inadvertently introduced at trace levels during growth or they may be deliberately added during growth or during subsequent diffusion treatments. Some point defects lead to increased light emission by participating in highly efficient radiative recombination paths while other defects introduce unwanted optical absorption bands that decrease the intensity of the light propagating through or emitted from the crystal. Electron paramagnetic resonance (EPR) and electron-nuclear double resonance (ENDOR) techniques[14] are well suited to identify and characterize paramagnetic point defects in bulk crystals such as $Li_2B_4O_7$. Information from hyperfine interactions is especially useful in developing specific models for point defects. Thus far, EPR studies in $Li_2B_4O_7$ have focused on Cu^{2+}, Co^{2+}, and Mn^{2+} impurities substituting for lithium[15–17] and vacancy-related defects produced by neutron irradiation at room temperature.[18,19]

In the present paper, EPR and ENDOR are used to investigate isolated oxygen and lithium vacancies in single crystals of $Li_2B_4O_7$. We irradiate the crystals at 77 K with x-rays, and then take EPR and ENDOR data between 13 and 40 K without any intervening warming. The x-rays convert the nonparamagnetic vacancies in the as-grown crystals to

a)Author to whom correspondence should be addressed. Electronic mail: john.mcclory@afit.edu.

 © 2010 American Institute of Physics

paramagnetic charge states that are observable with EPR. No new defects are produced by the ionizing radiation; we only change the charge state of vacancies that were created during the growth of the crystal. Two dominant EPR spectra, representing trapped electrons and trapped holes, are present after an irradiation at 77 K. The S=1/2 electron center is formed during the x-ray irradiation when a pre-existing oxygen vacancy traps an electron (this electron is primarily localized on one boron ion neighboring the oxygen vacancy). At the same time, the S=1/2 hole center is formed when a pre-existing lithium vacancy stabilizes a hole (this hole is primarily localized on a neighboring oxygen ion with nearly equal hyperfine interactions with the two adjacent boron ions). Single crystals of the closely related optical material lithium triborate (LiB_3O_5) have been studied previously with EPR and ENDOR,[20,21] thus allowing us to compare the electronic ground states of the x-ray-induced paramagnetic electron and hole traps in the two crystals ($Li_2B_4O_7$ and LiB_3O_5). Similar studies have also been reported for electron and hole traps in β-BaB_2O_4 crystals.[22]

II. EXPERIMENTAL

The two single crystals of $Li_2B_4O_7$ used in the present investigation were grown by the Czochralski technique ($T_{melt} \approx 917$ °C) at the Institute of Physical Optics (L'viv, Ukraine). One crystal was enriched with ^{10}B (greater than 97.3%). The other crystal contained the natural abundances of boron (19.8% ^{10}B and 80.2% ^{11}B). Copper was an unintentional impurity in both crystals. The dimensions of the samples used in the EPR and ENDOR experiments were approximately $1 \times 5 \times 3$ mm^3. The $Li_2B_4O_7$ crystals have a tetragonal structure and belong to the $I4_1cd$ space group (the point group is 4mm) with lattice constants a=9.475 Å and c=10.283 Å at room temperature.[23–27] A unit cell contains 104 atoms (8 formula units). The basic repeating structural building block in this crystal is $(B_4O_9)^{6-}$.

A Bruker EMX spectrometer was used to take EPR data and a Bruker Elexsys E-500 spectrometer was used to take ENDOR data. These spectrometers operated near 9.48 GHz (the EPR and the ENDOR microwave cavities had slightly different resonant frequencies). Helium-gas-flow systems maintained the sample temperature in the 13–40 K range, and proton NMR gaussmeters provided values of the static magnetic field. A small Cr-doped MgO crystal was used to correct for the difference in magnetic field between the sample and the probe tips of the gaussmeters (the isotropic g value for Cr^{3+} in MgO is 1.9800). An x-ray tube (operating at 60 kV and 30 mA) was used to convert defects in the $Li_2B_4O_7$ crystals to their paramagnetic charge states. Irradiation times were 30 min. A sample was immersed in liquid nitrogen during the irradiation and then was quickly transferred, without warming, into the cold helium gas stream passing through the microwave cavity. The intensities of the x-ray-induced EPR spectra indicate that the combined concentration of oxygen and lithium vacancies participating in paramagnetic defects in our crystals is in the 2 to 5 ppm range. This estimate is based on comparisons with a calibrated weak pitch sample from Bruker.

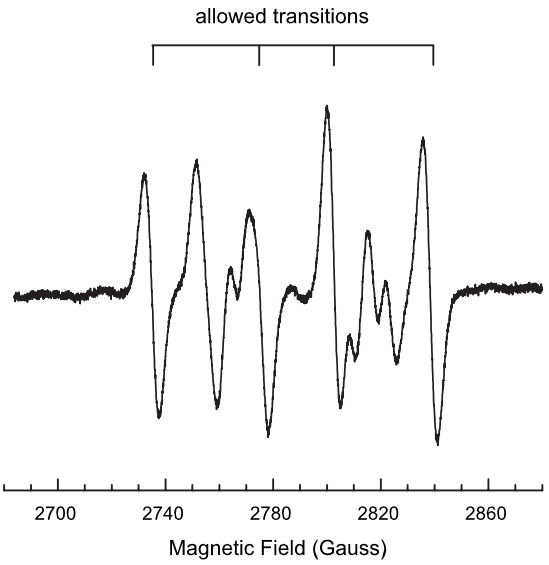

FIG. 1. EPR spectrum of Cu^{2+} ions substituting for lithium in a $Li_2B_4O_7$ crystal. These data were taken at 20 K with the magnetic field along the [001] direction. A large nuclear electric quadrupole interaction is responsible for the asymmetric appearance of the spectrum.

III. EPR AND ENDOR RESULTS

A. Cu^{2+} ions substituting for lithium ions

Figure 1 shows the EPR spectrum of Cu^{2+} ions in the unenriched $Li_2B_4O_7$ crystal. This spectrum was taken at 20 K with the magnetic field along the [001] direction after the crystal was irradiated at 77 K with x-rays. All of the crystallographically equivalent copper sites are magnetically equivalent for this orientation of magnetic field. Copper impurity ions substitute for lithium ions in the $Li_2B_4O_7$ lattice,[15] with most of them being in the monovalent charge state prior to the x-ray irradiation. These Cu^+ ($3d^{10}$) ions convert to Cu^{2+} ($3d^9$) ions during the irradiation as they trap "free" holes from the valence band. Heating above room temperature restores the preirradiation distribution of copper charge states. The spectrum in Fig. 1 is very sensitive to alignment of the magnetic field (misalignments of less than 0.1° produced observable site splittings). Because of this, the Cu^{2+} EPR spectrum was used to precisely align the magnetic field along the [001] direction in the studies of the electron and hole centers reported in this paper. The effective g value for the Cu^{2+} spectrum in $Li_2B_4O_7$ is 2.4302 ($\pm$0.0003) when the magnetic field is along the [001] direction. A recent EPR angular dependence study by Corradi *et al.*[15] provides complete **g** and **A** matrices for these Cu^{2+} ions.

Normally, an EPR spectrum from Cu^{2+} ions contains four equally spaced hyperfine lines due to the ^{63}Cu and ^{65}Cu isotopes. Both isotopes have I=3/2 and their nuclear magnetic moments are similar (^{63}Cu is 69.2% abundant and ^{65}Cu is 30.8% abundant). In many cases, signals from the two isotopes are resolved and eight lines (two similar sets of four lines) are observed in the EPR spectrum. The hyperfine pattern in Fig. 1, however, does not resemble a simple four-line hyperfine pattern because nuclear electric quadrupole interactions produce shifts in the allowed line positions and also introduce "forbidden" lines. With the magnetic field along

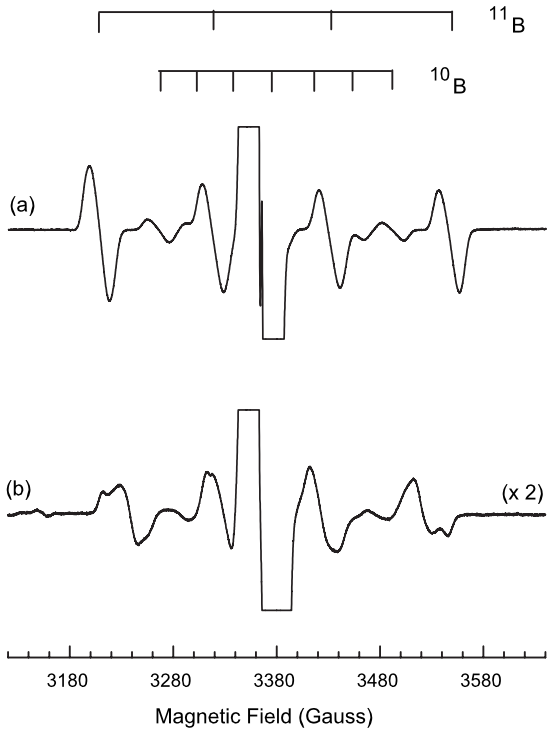

FIG. 2. EPR spectrum of the electron trap in the unenriched $Li_2B_4O_7$ crystal. The sample was irradiated at 77 K and the data were taken at 25 K. Stick diagrams indicate the ^{10}B and ^{11}B hyperfine lines in the upper spectrum. The off-scale signal near the center of the spectrum is due to trapped holes. (a) Magnetic field is along the [001] direction. (b) Magnetic field is along the [100] direction. The [100] spectrum has been multiplied by a factor of two to make it similar in intensity to the [001] spectrum.

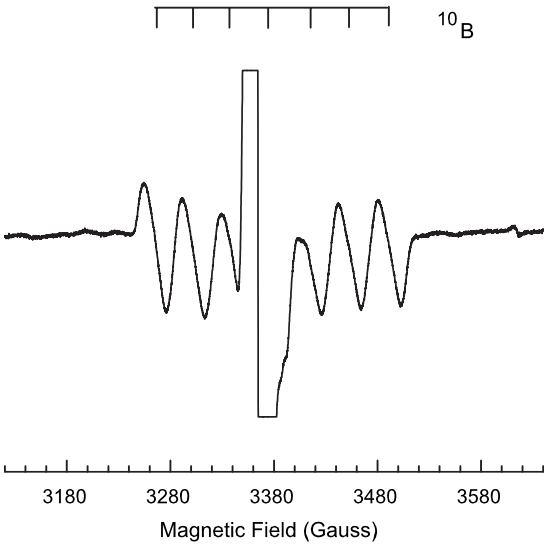

FIG. 3. EPR spectrum of the electron trap in the ^{10}B enriched $Li_2B_4O_7$ crystal. The crystal was irradiated at 77 K and the data were taken at 25 K with the magnetic field along the [001] direction. A stick diagram shows the ^{10}B hyperfine lines. The off-scale signal near the center of the spectrum is due to the trapped hole center.

the [001] direction in Fig. 1, allowed lines are at 2735, 2775, 2803, and 2838 G and forbidden lines appear between the first and second and the third and fourth allowed lines. For directions of the magnetic field other than those near [001], nuclear electric quadrupole effects are not easily observed in the Cu^{2+} spectra from $Li_2B_4O_7$ crystals because the hyperfine term in the spin Hamiltonian becomes considerably larger than the nuclear quadrupole term.

B. Electrons trapped at oxygen vacancies

Figure 2 shows EPR spectra obtained from the unenriched $Li_2B_4O_7$ crystal after an x-ray irradiation at 77 K. These data were taken at 25 K with the magnetic field along the [001] direction in Fig. 2(a) and along the [100] direction in Fig. 2(b). Following the irradiation at 77 K, the sample was immediately cooled to 25 K with no intermediate warming. The intense signal that goes off-scale near the middle of these spectra is due to a trapped hole (as discussed below in Sec. III C). In Fig. 2(a), four lines identified by the upper stick diagram are easily seen. They have an average separation between adjacent lines of 112.4 G and the magnetic field at their center corresponds to a g value of 2.0049 ($\pm$0.001). These four lines are caused by a hyperfine interaction with an I=3/2 nucleus, with the most likely candidate being a ^{11}B nucleus (80.2% abundant, I=3/2). Verification that this is the correct assignment comes from the observation of hyperfine lines from a ^{10}B nucleus (19.8% abundant, I=3). The outer two lines of a set of seven lines (illustrated by the second stick diagram) are found near 3265.4 and 3491.7 G in Fig. 2(a). The average separation between adjacent lines is 37.7 G in this set of seven lines. The ratio of the average separation in the set of four and the average separation in the set of seven is 2.98, which agrees with the expected ratio of 2.99 obtained from the known[28] nuclear magnetic moments of ^{11}B and ^{10}B.

In Fig. 2(b), the set of four EPR lines from the ^{11}B nucleus have an average separation of 94.1 G between adjacent lines. Additional structure, seen in Fig. 2(b) on the first and fourth lines of this set of four, is tentatively attributed to a weak hyperfine interaction with a nearby boron or lithium nucleus. The center of the four-line pattern in Fig. 2(b) corresponds to a g value of 2.0045 ($\pm$0.001), which is very close to the g value obtained for the spectrum in Fig. 2(a) when the estimated error limits are taken into account. A complete set of angular dependence data describing the four-line ^{11}B spectrum in Figs. 2(a) and 2(b) was not acquired in the present study because these EPR signals are relatively broad and it is difficult to accurately resolve the individual lines that arise from magnetically inequivalent sites of the responsible defect when the magnetic field is not along the crystal axes. Comparing the two spectra in Fig. 2 suggests that the g matrix and ^{11}B hyperfine matrix do not exhibit significant anisotropy, thus minimizing the need for an angular-dependence study.

Figure 3 shows the EPR spectrum obtained from the ^{10}B enriched $Li_2B_4O_7$ crystal after an x-ray irradiation at 77 K. These data were taken at 25 K with the magnetic field along the [001] direction. This enriched crystal contains very few ^{11}B nuclei and the x-ray-induced EPR spectrum is dominated by a set of seven equally spaced and equally intense lines due to the hyperfine interaction with one ^{10}B nucleus (I=3). The intense signal near the middle of the spectrum is again due to the trapped hole, but it now has a smaller width as a result of the ^{10}B enrichment. In Fig. 2(a), only the two outer

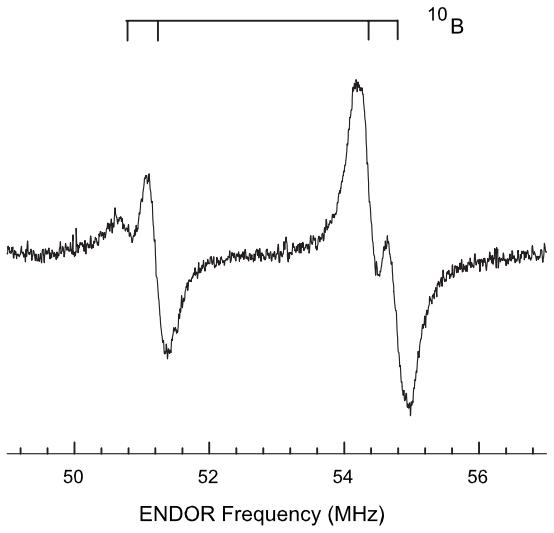

FIG. 4. ENDOR spectrum from the electron trap in the ^{10}B enriched $Li_2B_4O_7$ crystal. These data were taken at 13 K with the magnetic field along the [001] direction. The magnetic field was set at 3349.9 G, which corresponds to the third EPR line from the low-field end in Fig. 3.

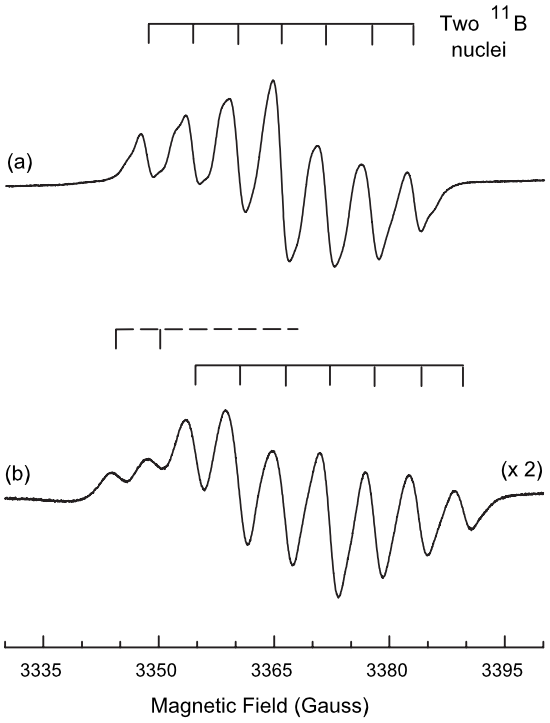

FIG. 5. EPR spectrum of the hole trap in the unenriched $Li_2B_4O_7$ crystal. The sample was irradiated at 77 K and the data were taken at 40 K. Stick diagrams show the ^{11}B hyperfine lines. (a) Magnetic field is along the [001] direction. (b) Magnetic field is along the [100] direction. This [100] spectrum has been multiplied by a factor of 2 to make it similar in intensity to the [001] spectrum.

lines of the seven-line ^{10}B pattern are easily observed, whereas in Fig. 3, six of the seven lines from the ^{10}B nuclei are well resolved. The average separation between adjacent lines is 37.8 G in Fig. 3 and the magnetic field at the center of the set of seven lines corresponds to a g value of 2.0036 ($\pm$0.001). Although this value agrees within experimental error with the g value for the four-line set in Fig. 2(a), its lower value suggests that the relaxed configuration of the defect, and thus the g value, may have a small isotope dependence (^{10}B versus ^{11}B). The unenriched sample in Fig. 2 and the ^{10}B enriched sample in Fig. 3 clearly show that the electron trap produced in $Li_2B_4O_7$ by ionizing radiation at low temperature has a dominant hyperfine interaction with one boron ion.

The ENDOR spectrum in Fig. 4 provides additional evidence that a ^{10}B nucleus is responsible for the set of seven hyperfine lines in Fig. 3. These ENDOR data in Fig. 4 were taken from the ^{10}B enriched crystal at 13 K with the magnetic field along the [001] direction, while holding the strength of the magnetic field at 3349.9 G (in the ENDOR cavity, this value of magnetic field corresponded to the third EPR line from the low-field side in Fig. 3). The four ENDOR lines in this spectrum occur at 50.78, 51.20, 54.42, and 54.72 MHz. The complete ENDOR spectrum from an $S=1/2$, $I=3$ spin system consists of 12 lines (two sets of six lines). The relative positions of these 12 lines provides information about the hyperfine parameter A, the nuclear electric quadrupole parameter P, and the "free" nuclear spin frequency ν_N (where $\nu_N=g_N\beta_N H/h$). For $A>\nu_N>P$, the 12 lines fall into two groups of six lines each. To first order, the two sets of six lines are offset from each other by $2\nu_N$ and the middle of the 12 lines is at A/2. The separations of the lines within a set of six are related to P. In our present case, the hyperfine pattern is well resolved in Fig. 3 and four out of the 12 lines are observed when ENDOR data is taken while sitting on the third EPR line. All 12 ENDOR lines are obtained by sequentially setting the magnetic field on each of the seven EPR lines in Fig. 3. This process gives lines at 50.34, 50.78, 51.20, 51.62, 52.03, and 52.48 MHz for the set of six at lower frequency and at 54.05, 54.39, 54.71, 55.07, 55.40, and 55.76 MHz for the set of six at higher frequency. These results include the four lines shown in Fig. 4. The average of the third and fourth lines in the lower set is 51.42 MHz and the average of the third and fourth lines in the higher set is 54.89 MHz. This places the middle of the 12 lines at 53.15 MHz, which when set equal to A/2 gives a value of 38.0 G for the hyperfine parameter A (this is very close to the 37.8 G splitting observed in the EPR spectrum in Fig. 3). The separation between the middle of the third and fourth lines in the lower set and the middle of the third and fourth lines in the higher set is 3.47 MHz. This represents an experimental estimate for $2\nu_N$. The known value of $2\nu_N$ for a ^{10}B nucleus is 3.07 MHz when the magnetic field is 3349.9 G (known values of ν_N at 3500 G for all magnetic nuclei are tabulated in Appendix A of Ref. 29). Allowing for second-order effects, our experimental estimate for $2\nu_N$ is close to the known value of $2\nu_N$ for ^{10}B, thus further verifying that a ^{10}B nucleus is responsible for the hyperfine splitting observed in the EPR spectrum in Fig. 3.

C. Holes stabilized by lithium vacancies

The EPR spectra in Fig. 5 are assigned to the radiation-induced trapped-hole center. These data were taken at 40 K from the unenriched $Li_2B_4O_7$ crystal after irradiating with x-rays at 77 K. The magnetic field is along the [001] direction in Fig. 5(a) and along the [100] direction in Fig. 5(b).

Although these trapped-hole center signals are present in Fig. 2, their structure is not seen in those spectra because the signals are distorted and are off-scale. By taking the spectra in Fig. 5 at 40 K instead of 25 K, we reduce microwave power saturation effects and clearly see the well-resolved structures that are associated with the trapped-hole center. In Fig. 5(a), a set of seven lines identified by the upper stick diagram are easily seen. They have an average separation between adjacent lines of 5.80 G and the magnetic field at their center corresponds to a g value of 2.0116 (±0.0001). These seven lines are caused by nearly equal hyperfine interactions with two I=3/2 nuclei (this results in seven equally spaced EPR lines with intensity ratios of 1:2:3:4:3:2:1). The ENDOR results presented later in this section show that two ^{11}B nuclei are responsible for the hyperfine structure in Fig. 5(a). EPR lines due to ^{10}B nuclei are not resolved in Fig. 5(a).

Two sets of seven EPR lines are observed when the magnetic field is along the [100] direction, as shown in Fig. 5(b). This spectrum indicates that there are two magnetically inequivalent sites for the trapped hole center for this direction of field. The complete higher-field set and two lines of the lower-field set are easily seen in Fig. 5(b), with the remaining five lines of the lower set hidden by the upper set. For the higher-field set, the average separation of lines is 5.81 G and the g value is 2.0083 (±0.0001). For the lower-field set, estimates of the average separation of lines and the g value are 4.79 G and 2.0161 (±0.0002), respectively. When comparing these latter two sets of numbers from Fig. 5(b) with the corresponding values of 5.80 G and 2.0116 obtained from Fig. 5(a), we see that the trapped hole center exhibits little anisotropy in either its hyperfine matrix or its g matrix. The three sets of seven lines in Fig. 5, with their small positive g shifts and their nearly isotropic hyperfine interactions, provide the critical information needed to construct a defect model for the trapped hole center. A complete set of angular dependence data was not acquired for this trapped-hole center because of the lack of resolution due to strongly overlapping lines.

Figure 6 shows ENDOR spectra obtained from the radiation-induced hole center in the unenriched $Li_2B_4O_7$ crystal. These data were taken at 25 K with the magnetic field along the [001] direction. They show that the two ^{11}B nuclei contributing to the hyperfine pattern in Fig. 5(a) are slightly inequivalent. In general, the complete ENDOR spectrum from an S=1/2, I_1=3/2, I_2=3/2 spin system consists of 12 lines if the hyperfine interactions are unequal (i.e., there are two sets of six lines, one set for each nucleus). In ENDOR spectra, each participating nucleus gives a set of lines representing that nucleus alone. Within a set of six lines for one nucleus, the lines divide into two groups of three. To first order when $A > \nu_N > P$, the middle lines of the two groups of three are separated by $2\nu_N$ and are centered on A/2. The separations within a group of three are related to P, the nuclear electric quadrupole parameter.

The four ENDOR traces in Fig. 6 were acquired while setting on the first, third, fifth, and seventh EPR lines in Fig. 5(a), when counting from low field. As illustrated by the upper stick diagrams, these four spectra contain six ENDOR lines (overlapping lines are present in the middle two spectra). A corresponding set of six lines appears in the region between 3 and 4 MHz. These lower frequency lines overlap ENDOR lines from ^{10}B nuclei and from distant ^{11}B nuclei and thus cannot be unambiguously identified. The six lines in Fig. 6 are separated into a set of three assigned to nucleus 1 (at 12.32, 12.44, and 12.59 MHz) and a set of three assigned to nucleus 2 (at 12.37, 12.47, and 12.64 MHz). Nucleus 1 and 2 are labels referring to the two nearly equivalent ^{11}B nuclei that are responsible for the seven-line EPR hyperfine pattern in Fig. 5(a). A nuclear electric quadrupole interaction causes the splitting within each set of three ENDOR lines in Fig. 6, while the small shift of the two sets of ENDOR lines relative to each other is a direct measure of slight inequivalency of the two ^{11}B nuclei. If the two ^{11}B nuclei had equal hyperfine interactions for this [001] direction of magnetic field, the ENDOR spectra in Fig. 6 would consist of one set of three lines (with double the intensities). The separation of 30 kHz between the two center lines in Fig. 6, when compared to the A/2 value of 8.1 MHz (half of 5.80 G), suggests that there is less than 0.4% difference in the hyperfine interactions for the two ^{11}B nuclei participating in the EPR spectrum in Fig. 5(a).

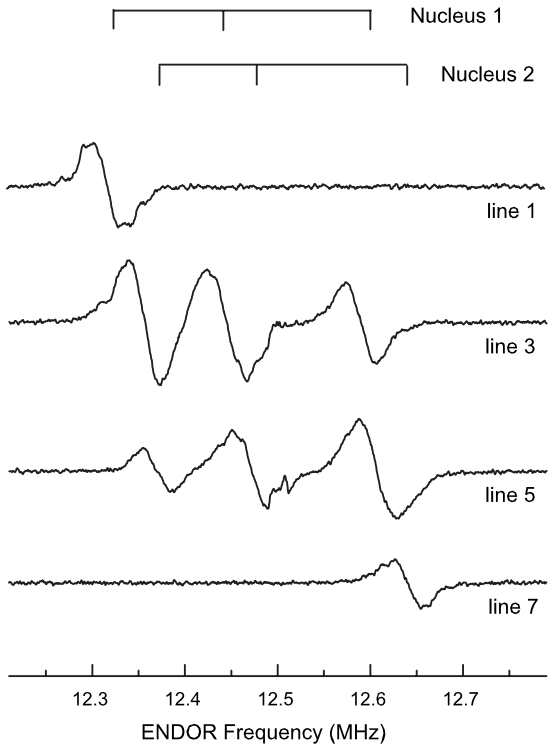

FIG. 6. ENDOR spectrum from the hole trap in the unenriched $Li_2B_4O_7$ crystal. These data were taken at 25 K with the magnetic field along the [001] direction. As indicated above, the four ENDOR spectra were taken while holding the magnetic field at the first, third, fifth, and seventh EPR lines in Fig. 5(a), when counting from low-field.

The EPR spectrum from the trapped-hole center in the ^{10}B enriched $Li_2B_4O_7$ crystal is shown in Fig. 7. These data were taken at 40 K with the magnetic field along the [001] direction. Instead of seven hyperfine lines from two nearly equivalent ^{11}B nuclei (each with I=3/2), the EPR spectrum should now have 13 equally spaced hyperfine lines from two nearly equivalent ^{10}B nuclei (each with I=3). These lines

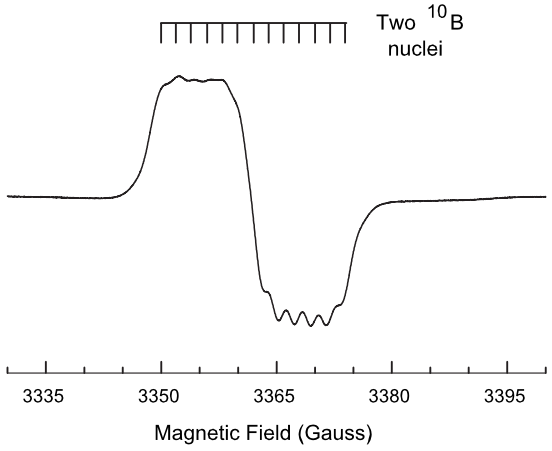

FIG. 7. EPR spectrum of the hole trap in the ^{10}B enriched $Li_2B_4O_7$ crystal. The crystal was irradiated at 77 K and the data were taken at 40 K with the magnetic field along the [001] direction. A stick diagram shows the 13 ^{10}B hyperfine lines.

will have intensity ratios of 1:2:3:4:5:6:7:6:5:4:3:2:1. The separation between adjacent lines in this set of 13 is expected to be approximately 1.94 G [i.e., the 5.80 G separation in Fig. 5(a) is reduced by the 2.99 ratio of the boron magnetic moments]. This predicts an overall width of approximately 23.3 G for the trapped hole center in the ^{10}B enriched sample. In agreement with these expectations, we see that the width of the EPR spectrum in Fig. 7 is approximately 25 G. Furthermore, the partially resolved structure on the high field side of this spectrum has separations of about 2 G between adjacent lines. The measured g value for the EPR spectrum in Fig. 7 is 2.0116 ($\pm$0.0002).

Figure 8 shows an ENDOR spectrum from the trapped-hole center in the ^{10}B enriched $Li_2B_4O_7$ crystal. These data were taken at 28 K with the magnetic field parallel to the [001] direction. The field was held at 3375.7 G (in the ENDOR cavity, this value of magnetic field corresponded to the center of the EPR spectrum in Fig. 7). The four lines in Fig. 8 at 4.12, 4.18, 4.26, and 4.35 MHz are due to ^{10}B nuclei. Their linewidths are approximately 40 kHz. Corresponding

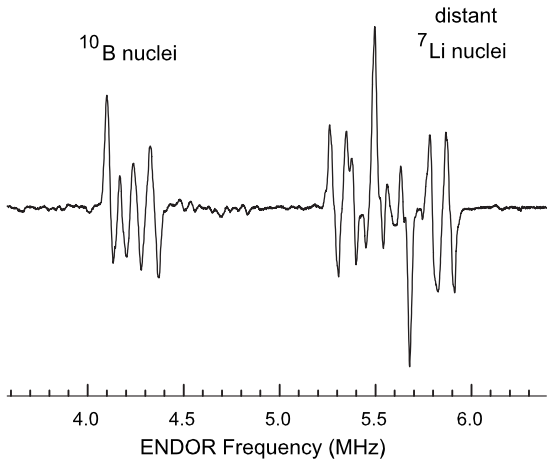

FIG. 8. ENDOR spectrum from the hole trap in the ^{10}B enriched $Li_2B_4O_7$ crystal. These data were taken at 28 K with the magnetic field along the [001] direction. The magnetic field was set at 3375.7 G, which in the ENDOR cavity corresponded to the middle of the EPR spectrum in Fig. 7.

lower-frequency lines are expected near 1.1 MHz, but they are not easily distinguished from other ENDOR lines appearing in that region. The complete ENDOR spectrum from an $S=1/2$, $I_1=3$, $I_2=3$ spin system consists of 24 lines if the two hyperfine interactions are unequal (i.e., there would be two sets of 12 lines, one set for each nucleus). Our results in Fig. 8 indicate that the two ^{10}B hyperfine interactions are very similar and give rise to only one set of six lines near 4.2 MHz and another set of six lines near 1.1 MHz. Small separations of lines are not observed in Fig. 8 that would show the two ^{10}B nuclei have slightly inequivalent interactions. An extrapolation of the ^{11}B results in Fig. 6 suggests that these expected separations from inequivalent nuclei in Fig. 8 are less than the experimental linewidths. Thus a maximum of six lines with spacings related to the nuclear electric quadrupole interaction should be found in the 4.2 MHz region. Although it is not initially obvious, all six of these expected ^{10}B lines are present in Fig. 8. Acquiring ENDOR spectra while setting at different values of magnetic field across the broad EPR signal in Fig. 7 demonstrates that the first and fourth ^{10}B ENDOR signals in Fig. 8 each represent two very closely spaced lines. The nuclear electric quadrupole moment of a ^{10}B nucleus is 2.15 times larger than the nuclear electric quadrupole moment of a ^{11}B nucleus. This makes the nuclear electric quadrupole term in the spin Hamiltonian closer in magnitude to the hyperfine and nuclear Zeeman terms for the trapped hole center in the ^{10}B enriched crystal, and thus leads to the more complicated quadrupole pattern for the ^{10}B nuclei appearing in Fig. 8.

The ^{10}B ENDOR results in Fig. 8 and the ^{11}B ENDOR results in Fig. 6 agree with each other and together show that the two boron nuclei neighboring the trapped hole have similar hyperfine interactions (i.e., they are nearly equivalent). An additional group of ENDOR lines at higher frequency in Fig. 8 shows that neighboring lithium ions do not play a primary role in the trapped-hole center. This group of ENDOR lines is centered on 5.58 MHz in Fig. 8, and the known value[29] of ν_N for ^{7}Li is 5.586 MHz when the magnetic field is 3375.7 G. This good agreement between the known value of ν_N and the measured center frequency of these lines between 5 and 6 MHz conclusively shows that ^{7}Li is the responsible nucleus. The hyperfine interactions represented by these lines are very small (less than 0.6 MHz), which indicates that they are due to "distant" ^{7}Li nuclei located several lattice spaces away from the trapped hole. There are no observable ENDOR lines in our spectra that could be assigned to lithium ions interacting closely with the unpaired electron spin of the trapped hole center.

IV. DISCUSSION

In $Li_2B_4O_7$ crystals, oxygen vacancies and lithium vacancies charge compensate each other and are simultaneously formed during growth. When a $Li_2B_4O_7$ crystal is irradiated at 77 K with 60 kV x-rays, a portion of these vacancies stabilize (i.e., trap) "free" electrons and holes and form the paramagnetic defects that are observed with EPR. The radiation-induced electron and hole centers remain stable in the crystal after an irradiation as long as it is held at

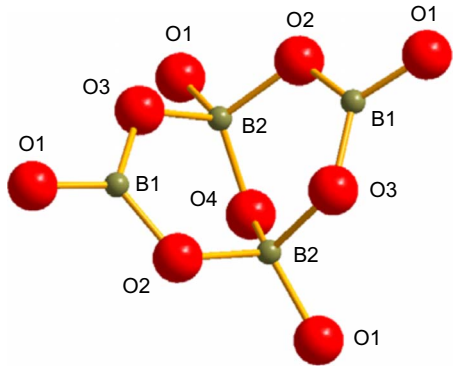

FIG. 9. (Color online) Schematic representation of the basic (B_4O_9) structural building block in $Li_2B_4O_7$ crystals. This is an arbitrary projection chosen to best illustrate the two BO_3 units and two BO_4 units. The labeling scheme used to identify the boron and oxygen ions in this figure is also used in Table I.

a temperature below 77 K. When the crystal is warmed above the irradiation temperature, holes are released from their trapping sites near the lithium vacancies and recombine with the electrons localized at the oxygen vacancies. The trapped holes become thermally unstable near 90 K, and the EPR signals associated with the oxygen and lithium vacancies quickly disappear when the sample is briefly taken above this temperature. The sample must be irradiated again at 77 K to restore the EPR signals. As expected, we found that the same trapped electron and trapped hole defects were produced in the unenriched and the ^{10}B enriched $Li_2B_4O_7$ crystals when irradiated at 77 K with x-rays.

The boron hyperfine interactions observed in our EPR and ENDOR spectra combined with the known crystal structure of $Li_2B_4O_7$ allow us to suggest specific models for the x-ray-induced trapped-electron and trapped-hole centers. Figure 9 shows a schematic representation of the basic $(B_4O_9)^{6-}$ building block occurring in the $Li_2B_4O_7$ lattice, with its two BO_3 units and two BO_4 units. The arbitrary projection plane in Fig. 9 was chosen to best illustrate the linkages between these BO_3 and BO_4 units. The BO_3 units, with shorter B–O bond lengths, consist of a B_1 ion surrounded by O_1, O_2, and O_3 ions, while the BO_4 units, with longer B–O bond lengths, consist of a B_2 ion surrounded by O_1, O_2, O_3, and O_4 ions. Every oxygen ion has two boron neighbors in the $Li_2B_4O_7$ lattice (i.e., they are all bridging oxygen ions). The O_1, O_2, and O_3 ions link B_1 and B_2 ions, while the O_4 ion links two B_2 ions. Table I lists the B–O bond lengths appearing in Fig. 9, and also includes the Li–O separation distances.[26,27]

TABLE I. B–O bond lengths and Li–O separation distances at low temperature in the $Li_2B_4O_7$ lattice. Results from two recent crystallographic studies are included.

	Bond lengths and separation distances (Å)	
	(From Ref. 26)	(From Ref. 27)
B_1-O_1	1.351	1.363
B_1-O_2	1.369	1.379
B_1-O_3	1.374	1.379
B_2-O_1	1.454	1.452
B_2-O_2	1.508	1.526
B_2-O_3	1.500	1.503
B_2-O_4	1.451	1.445
$Li-O_1$	2.115	2.161
$Li-O_2$	1.970	2.022
$Li-O_3$	2.019	1.998
$Li-O_3$	2.064	2.048
$Li-O_4$	2.643	2.595

A. Model of the trapped-electron center

The most characteristic feature of the trapped-electron center in $Li_2B_4O_7$ is the large, and nearly isotropic, hyperfine interaction with one boron neighbor. As shown in Fig. 2 for the unenriched sample, the four-line ^{11}B hyperfine pattern has 112.4 and 94.1 G separations when the magnetic field is along the [001] and [100] directions, respectively. These values, which are much larger than the ^{11}B hyperfine separations occurring in the trapped-hole center, indicate that a significant amount of the unpaired electron occupies a hybridized 2*s* and 2*p* orbital centered on the primary boron ion.[30,31] This localization of the trapped electron on a boron would occur if the boron ion is adjacent to an oxygen vacancy. It has previously been observed that an oxygen vacancy in lithium triborate (LiB_3O_5) crystals traps an electron and forms an EPR spectrum with one dominant ^{11}B hyperfine interaction.[20,21] Now, a similar behavior is seen in $Li_2B_4O_7$ crystals.

When refining the model of the electron center in $Li_2B_4O_7$, the questions are which of the two boron ions, B_1 or B_2, is responsible for the large hyperfine interaction and which of the neighboring oxygen ions is missing. A series of first-principles calculations that identify the minimum-energy configuration of the singly ionized oxygen vacancy may help answer these questions. Meanwhile, we provide simple electrostatics arguments that suggest specific answers. The BO_3 units have less negative charge (fewer oxygen ions) and will not repel a trapped electron as much as a BO_4 unit. Also, the BO_3 units have shorter bond lengths than the BO_4 units (see Fig. 9 and Table I). Thus, an oxygen vacancy in a BO_3 unit will be closer to the electron localized on the boron ion (more precisely, on the BO_2 unit that remains after the third oxygen ion is removed) and this extra electron will be more tightly bound (i.e., have lower total energy). For these reasons, we suggest that the unpaired spin associated with the trapped-electron center in $Li_2B_4O_7$ crystals has its large hyperfine interaction with a B_1 ion and the oxygen vacancy is at the neighboring O_1 position. The B_1-O_1 bond length is slightly smaller than the B_1-O_2 and B_1-O_3 bond lengths. We recognize that lattice relaxations will play an important role in determining the ionic structure of the ground state of an oxygen vacancy in $Li_2B_4O_7$. In this regard, we draw attention to the well-known E_1' center[32,33] in crystalline SiO_2 where an asymmetric relaxation causes the unpaired electron to be primarily localized on only one of the two silicon ions adjacent to the oxygen vacancy.

B. Model of the trapped-hole center

The trapped-hole center in $Li_2B_4O_7$ has nearly equal hyperfine interactions with two adjacent boron nuclei. As

shown in Fig. 5(a), the seven-line ^{11}B hyperfine pattern for the unenriched sample has separations of 5.8 G when the magnetic field is along the [001] direction. These hyperfine interactions with boron nuclei are significantly smaller than the boron hyperfine interaction observed in the trapped-electron center, which suggests that the unpaired spin associated with the trapped-hole center is not primarily localized on the boron ions. In nearly all insulating oxide crystals, it is well-known that trapped holes are localized on oxygen ions with only small hyperfine interactions with the neighboring cations. These hole centers are formed when a substitutional O^{2-} ion traps a hole and becomes an O^- ion (the resulting unpaired spin occupies an oxygen *p* orbital). In most cases, either an adjacent cation vacancy or a nearby impurity on a cation site provides the needed electrostatic attraction that stabilizes the hole on the oxygen ion. Trapped-hole centers of this type are readily found in simple oxides such as MgO, ZnO, and SiO_2.[34–36] A relevant example for the present study is a hole trapped on an oxygen ion within a BO_4 unit that is formed when a boron ion substitutes for a silicon ion in a SiO_4 unit in zircon ($ZrSiO_4$).[37]

The requirement that the hole trapped on an oxygen ion interacts nearly equally with two boron ions restricts the possible models for this defect in $Li_2B_4O_7$. According to Fig. 9 and Table I, every oxygen ion in the $Li_2B_4O_7$ lattice has two boron neighbors. The O_1, O_2, and O_3 ions have B_1 and B_2 ions as nearest neighbors and the O_4 ions have two B_2 ions as nearest neighbors. The B_2-O bonds in the BO_4 units are longer than the B_1-O bonds in the BO_3 units. A simple electrostatics argument suggests that the hole will be trapped on the oxygen ion linking two BO_4 units. The positive hole on the oxygen ion is repelled by the positive boron ions and thus the total energy of the defect is minimized when the B–O separation distances are greatest (the remaining oxygen ions around the boron ions help to reduce this repulsive effect). Another supporting argument comes from the fact that the oxygen ion that links two BO_4 units is equidistant from its two neighboring boron ions. This should give rise to hyperfine interactions that are nearly equal, and thus in agreement with experiment. For these reasons, we suggest a model for the trapped-hole center in $Li_2B_4O_7$ crystals that has the hole localized in a nonbonding *p* orbital on an O_4 oxygen ion and has equivalent hyperfine interactions with the two adjacent B_2 boron ions.

The small positive shifts observed in the g values for the trapped-hole center are in agreement with this model of a hole trapped in a nonbonding *p* orbital on an oxygen ion. Three discrete energy levels (E_1, E_2, and E_3, in ascending order) are produced when the threefold orbital degeneracy of this ^2P state ($L=1, S=1/2$) is removed by the crystalline electric field. Spin-orbit interactions mix these excited states with the ground state and give the following first-order expressions for the expected principal g values.[21]

$$g_1 = g_e, \tag{1}$$

$$g_2 = g_e - \frac{2\lambda}{E_3 - E_1}, \tag{2}$$

$$g_3 = g_e - \frac{2\lambda}{E_2 - E_1}. \tag{3}$$

The spin-orbit coupling constant λ for an O^- ion is $-135\ cm^{-1}$. A negative sign for λ gives rise to positive g shifts. In general, a hole trapped on an oxygen ion has g values that vary from 2.003 to 2.050.[34–37] Our measured g values, reported in Sec. III C, are within this expected range. The energy differences E_3-E_1 and E_2-E_1 appearing in the denominators in Eqs. (2) and (3) correspond to visible and near-infrared optical absorption bands associated with the trapped-hole center. These broad absorption bands are responsible for the brownish color of the $Li_2B_4O_7$ crystals that is present immediately after irradiating at low temperature with x-rays. The crystals are clear to the eye before an irradiation, and the singly ionized oxygen vacancies are expected to have one or more optical absorption bands in the ultraviolet.[20]

The "effective" negative charge of a nearby lithium vacancy stabilizes the hole on the O_4 oxygen ion. As indicated in Table I, a lithium ion is approximately 2.6 Å from the O_4 ion. Other oxygen ions (O_1, O_2, and O_3) are closer to lithium sites, but the reduction in the total energy of the hole because a negative lithium vacancy is closer may be more than offset by the increase in the energy of the hole because the positive B_1 ion is also closer. The 90 K decay temperature of the hole center suggests that it is a shallow trap, and this is consistent with a well-separated lithium vacancy providing the stabilization energy. Relaxations of the ions participating in the defect may also contribute to the stabilization energy. A relevant example is the trapped-hole center in LiB_3O_5 crystals where a large hyperfine interaction is observed with only one boron ion and the effect of lattice relaxation is shown to play a major role in the ionic structure of the ground state.[21]

V. SUMMARY

Oxygen and lithium vacancies are both present in as-grown $Li_2B_4O_7$ crystals. During an irradiation at 77 K with x-rays, electrons are trapped at the oxygen vacancies and holes are stabilized by the lithium vacancies. This produces two distinct $S=1/2$ paramagnetic spectra that can be monitored in EPR and ENDOR experiments. Hyperfine interactions with ^{10}B and ^{11}B nuclei allow us to suggest models for these defects. The electron trap has the electron localized on a boron ion in a BO_3 unit that contains an oxygen vacancy (i.e., the electron is trapped by the remaining BO_2 unit). This gives rise to a large hyperfine interaction with one boron ion. The hole trap has the hole localized in a nonbonding *p* orbital on an oxygen ion that serves as the bridge between two BO_4 units. This gives rise to smaller, and nearly equal, hyperfine interactions with the two boron ions in the adjoining BO_4 units. First-principles calculations will help establish more detailed models for these basic trapped-electron and trapped-hole centers in $Li_2B_4O_7$ crystals.

ACKNOWLEDGMENTS

This work was supported at the Air Force Institute of Technology by Grant Nos. HDTRA1-07-1-0008 and

BRBAA08-I-2-0128 from the Defense Threat Reduction Agency and at West Virginia University by Grant No. DMR-0804352 from the National Science Foundation. The views expressed in this article are those of the authors and do not necessarily reflect the official policy or position of the Air Force, the Department of Defense, or the United States Government.

[1]T. Sugawara, R. Komatsu, and S. Uda, Solid State Commun. **107**, 233 (1998).
[2]V. Petrov, F. Rotermund, F. Noack, R. Komatsu, T. Sugawara, and S. Uda, J. Appl. Phys. **84**, 5887 (1998).
[3]P. Kumbhakar and T. Kobayashi, Appl. Phys. B: Lasers Opt. **78**, 165 (2004).
[4]M. Martini, F. Meinardi, L. Kovacs, and K. Polgar, Radiat. Prot. Dosim. **65**, 343 (1996).
[5]M. Prokic, Radiat. Prot. Dosim. **100**, 265 (2002).
[6]N. Can, T. Karali, P. D. Townsend, and F. Yildiz, J. Phys. D **39**, 2038 (2006).
[7]Y. V. Burak, V. T. Adamiv, I. M. Teslyuk, and V. M. Shevel, Radiat. Meas. **38**, 681 (2004).
[8]T. Shiosaki, M. Adachi, H. Kobayashi, K. Araki, and A. Kawabata, Jpn. J. Appl. Phys., Suppl. 1 **24**, 25 (1985).
[9]A. Ballato, J. Kosinski, and T. Lukaszek, IEEE Trans. Ultrason. Ferroelectr. Freq. Control **38**, 62 (1991).
[10]M. Maeda, H. Tachi, K. Honda, and I. Suzuki, Jpn. J. Appl. Phys., Part 1 **33**, 1965 (1994).
[11]A. S. Bhalla, L. E. Cross, and R. W. Whatmore, Jpn. J. Appl. Phys., Suppl. 2, **24**, 727 (1985).
[12]I. Ketsman, D. Wooten, J. Xiao, Y. B. Losovyj, Y. V. Burak, V. T. Adamiv, A. Sokolov, J. Petrosky, J. McClory, and P. A. Dowben, Phys. Lett. A **374**, 891 (2010).
[13]D. Wooten, I. Ketsman, J. Xiao, Y. B. Losovyj, J. Petrosky, J. McClory, Y. V. Burak, V. T. Adamiv, and P. A. Dowben, Physica B **405**, 461 (2010).
[14]J.-M. Spaeth and H. Overhof, *Point Defects in Semiconductors and Insulators: Determination of Atomic and Electronic Structure from Paramagnetic Hyperfine Interactions* (Springer-Verlag, Heidelberg, 2003).
[15]C. Corradi, V. Nagirnyi, A. Kotlov, A. Watterich, M. Kirm, K. Polgar, A. Hofstaetter, and M. Meyer, J. Phys.: Condens. Matter **20**, 025216 (2008).
[16]D. Piwowarska, S. M. Kaczmarek, M. Berkowski, and I. Stefaniuk, J. Cryst. Growth **291**, 123 (2006).
[17]D. Podgorska, S. M. Kaczmarek, W. Drozdowski, M. Wabia, M. Kwasny, S. Warchol, and V. M. Rizak, Mol. Phys. Rep. **39**, 199 (2004).
[18]G. I. Malovichko, V. G. Grachev, and A. O. Matkovskii, Sov. Phys. Solid State **33**, 1107 (1991).
[19]Y. V. Burak, B. V. Padlyak, and V. M. Shevel, Radiat. Eff. Defects Solids **157**, 1101 (2002).
[20]M. P. Scripsick, X. H. Fang, G. J. Edwards, L. E. Halliburton, and J. K. Tyminski, J. Appl. Phys. **73**, 1114 (1993).
[21]W. Hong, M. M. Chirila, N. Y. Garces, L. E. Halliburton, D. Lupinski, and P. Villeval, Phys. Rev. B **68**, 094111 (2003).
[22]W. Hong, L. E. Halliburton, K. T. Stevens, D. Perlov, G. C. Catella, R. K. Route, and R. S. Feigelson, J. Appl. Phys. **94**, 2510 (2003).
[23]J. Krogh-Moe, Acta Crystallogr. **15**, 190 (1962).
[24]J. Krogh-Moe, Acta Crystallogr., Sect. B: Struct. Crystallogr. Cryst. Chem. **24**, 179 (1968).
[25]S. F. Radaev, L. A. Muradyan, L. F. Malakhova, Y. V. Burak, and V. I. Simonov, Kristallografiya **34**, 1400 (1989).
[26]N. Sennova, R. S. Bubnova, G. Cordier, B. Albert, S. K. Filatov, and L. Isaenko, Z. Anorg. Allg. Chem. **634**, 2601 (2008).
[27]V. T. Adamiv, Y. V. Burak, and I. M. Teslyuk, J. Alloys Compd. **475**, 869 (2009).
[28]J. A. Weil and J. R. Bolton, *Electron Paramagnetic Resonance: Elementary Theory and Practical Applications*, 2nd ed. (Wiley, Hoboken, New Jersey, 2007), p. 581.
[29]J.-M. Spaeth, J. R. Niklas, and R. H. Bartram, *Structural Analysis of Point Defects in Solids: An Introduction to Multiple Magnetic Resonance Spectroscopy* (Springer-Verlag, Berlin, 1992), pp. 329–332.
[30]J. R. Morton and K. F. Preston, J. Magn. Reson. (1969–1992) **30**, 577 (1978).
[31]J. A. J. Fitzpatrick, F. R. Manby, and C. M. Western, J. Chem. Phys. **122**, 084312 (2005).
[32]J. K. Rudra and W. B. Fowler, Phys. Rev. B **35**, 8223 (1987).
[33]M. Boero, A. Pasquarello, J. Sarnthein, and R. Car, Phys. Rev. Lett. **78**, 887 (1997).
[34]Y. Chen and M. M. Abraham, J. Phys. Chem. Solids **51**, 747 (1990).
[35]O. F. Schirmer, J. Phys. Chem. Solids **29**, 1407 (1968).
[36]R. H. D. Nuttall and J. A. Weil, Can. J. Phys. **59**, 1696 (1981).
[37]C. J. Walsby, N. S. Lees, W. C. Tennant, and R. F. C. Claridge, J. Phys.: Condens. Matter **12**, 1441 (2000).